Associative Embedding:
End-to-End Learning for Joint Detection and Grouping

Alejandro Newell
University of Michigan
alnewell@umich.edu

Zhiao Huang*
Tsinghua University
hza14@mails.tsinghua.edu.cn

Jia Deng
University of Michigan
jiadeng@umich.edu

Abstract

We introduce associative embedding, a novel method for supervising convolutional neural networks for the task of detection and grouping. A number of computer vision problems can be framed in this manner including multi-person pose estimation, instance segmentation, and multi-object tracking. Usually the grouping of detections is achieved with multi-stage pipelines, instead we propose an approach that teaches a network to simultaneously output detections and group assignments. This technique can be easily integrated into any state-of-the-art network architecture that produces pixel-wise predictions. We show how to apply this method to both multi-person pose estimation and instance segmentation and report state-of-the-art performance for multi-person pose on the MPII and MS-COCO datasets.

1. Introduction

Many computer vision tasks can be viewed as joint detection and grouping: detecting smaller visual units and grouping them into larger structures. For example, multi-person pose estimation can be viewed as detecting body joints and grouping them into individual people; instance segmentation can be viewed as detecting relevant pixels and grouping them into object instances; multi-object tracking can be viewed as detecting object instances and grouping them into tracks. In all of these cases, the output is a variable number of visual units and their assignment into a variable number of visual groups.

Such tasks are often approached with two-stage pipelines that perform detection first and grouping second. But such approaches may be suboptimal because detection and grouping are usually tightly coupled: for example, in multiperson pose estimation, a wrist detection is likely a false positive if there is not an elbow detection nearby to group with.

In this paper we ask whether it is possible to jointly perform detection and grouping using a single-stage deep net-

Figure 1. Both multi-person pose estimation and instance segmentation are examples of computer vision tasks that require detection of visual elements (joints of the body or pixels belonging to a semantic class) and grouping of these elements (as poses or individual object instances).

work trained end-to-end. We propose *associative embedding*, a novel method to represent the output of joint detection and grouping. The basic idea is to introduce, for each detection, a real number that serves as a "tag" to identify the group the detection belongs to. In other words, the tags associate each detection with other detections in the same group.

Consider the special case of detections in 2D and embeddings in 1D (real numbers). The network outputs both a heatmap of per-pixel detection scores and a heatmap of per-pixel identity tags. The detections and groups are then decoded from these two heatmaps.

To train a network to predict the tags, we use a loss function that encourages pairs of tags to have similar values if the corresponding detections belong to the same group in the ground truth or dissimilar values otherwise. It is important to note that we have no "ground truth" tags for the network to predict, because what matters is not the particular tag values, only the differences between them. The network has the freedom to decide on the tag values as long as they agree with the ground truth grouping.

We apply our approach to multiperson pose estimation, an important task for understanding humans in images. Concretely, given an input image, multi-person pose estimation

---

* Work done while a visiting student at the University of Michigan.

seeks to detect each person and localize their body joints. Unlike single-person pose there are no prior assumptions of a person's location or size. Multi-person pose systems must scan the whole image detecting all people and their corresponding keypoints. For this task, we integrate associative embedding with a stacked hourglass network [31], which produces a detection heatmap and a tagging heatmap for each body joint, and then groups body joints with similar tags into individual people. Experiments demonstrate that our approach outperforms all recent methods and achieves state of the art results on MS-COCO [27] and MPII Multiperson Pose [3, 35].

We further demonstrate the utility of our method by applying it to instance segmentation. Showing that it is straightforward to apply associative embedding to a variety of vision tasks that fit under the umbrella of detection and grouping.

Our contributions are two fold: (1) we introduce associative embedding, a new method for single- stage, end-to-end joint detection and grouping. This method is simple and generic; it works with any network architecture that produces pixel-wise prediction; (2) we apply associative embedding to multiperson pose estimation and achieve state of the art results on two standard benchmarks.

2. Related Work

Vector Embeddings Our method is related to many prior works that use vector embeddings. Works in image retrieval have used vector embeddings to measure similarity between images [17, 53]. Works in image classification, image captioning, and phrase localization have used vector embeddings to connect visual features and text features by mapping them to the same vector space [16, 20, 30]. Works in natural language processing have used vector embeddings to represent the meaning of words, sentences, and paragraphs [39, 32]. Our work differs from these prior works in that we use vector embeddings as identity tags in the context of joint detection and grouping.

Perceptual Organization Work in perceptual organization aims to group the pixels of an image into regions, parts, and objects. Perceptual organization encompasses a wide range of tasks of varying complexity from figure-ground segmentation [37] to hierarchical image parsing [21]. Prior works typically use a two stage pipeline [38], detecting basic visual units (patches, superpixels, parts, etc.) first and grouping them second. Common grouping approaches include spectral clustering [51, 46], conditional random fields (e.g. [31]), and generative probabilistic models (e.g. [21]). These grouping approaches all assume pre-detected basic visual units and pre-computed affinity measures between them but differ among themselves in the process of converting affinity measures into groups. In contrast, our approach performs detection and grouping in one stage using a generic network that includes no special design for grouping.

It is worth noting a close connection between our approach to those using spectral clustering. Spectral clustering (e.g. normalized cuts [46]) techniques takes as input precomputed affinities (such as predicted by a deep network) between visual units and solves a generalized eigenproblem to produce embeddings (one per visual unit) that are similar for visual units with high affinity. Angular Embedding [37, 47] extends spectral clustering by embedding depth ordering as well as grouping. Our approach differs from spectral clustering in that we have no intermediate representation of affinities nor do we solve any eigenproblems. Instead our network directly outputs the final embeddings.

Our approach is also related to the work by Harley et al. on learning dense convolutional embeddings [24], which trains a deep network to produce pixel-wise embeddings for the task of semantic segmentation. Our work differs from theirs in that our network produces not only pixelwise embeddings but also pixel-wise detection scores. Our novelty lies in the integration of detection and grouping into a single network; to the best of our knowledge such an integration has not been attempted for multiperson human pose estimation.

Multiperson Pose Estimation Recent methods have made great progress improving human pose estimation in images in particular for single person pose estimation [50, 48, 52, 40, 8, 5, 41, 4, 14, 19, 34, 26, 7, 49, 44]. For multiperson pose, prior and concurrent work can be categorized as either top-down or bottom-up. Top-down approaches [42, 25, 15] first detect individual people and then estimate each person's pose. Bottom-up approaches [45, 28, 29, 6] instead detect individual body joints and then group them into individuals. Our approach more closely resembles bottom-up approaches but differs in that there is no separation of a detection and grouping stage. The entire prediction is done at once by a single-stage, generic network. This does away with the need for complicated post-processing steps required by other methods [6, 28].

Instance Segmentation Most existing instance segmentation approaches employ a multi-stage pipeline to do detection followed by segmentation [23, 18, 22, 11]. Dai et al. [12] made such a pipeline differentiable through a special layer that allows backpropagation through spatial coordinates.

Two recent works have sought tighter integration of detection and segmentation using fully convolutional networks. DeepMask [43] densely scans subwindows and outputs a detection score and a segmentation mask (reshaped to a vector) for each subwindow. Instance-Sensitive FCN [10] treats each object as composed of a set of object parts in a regular grid, and outputs a per-piexl heatmap of detection scores for each object part. Instance-Sensitive FCN (IS-FCN) then detects object instances where the part detection scores are spaitally coherent, and assembles object masks from the
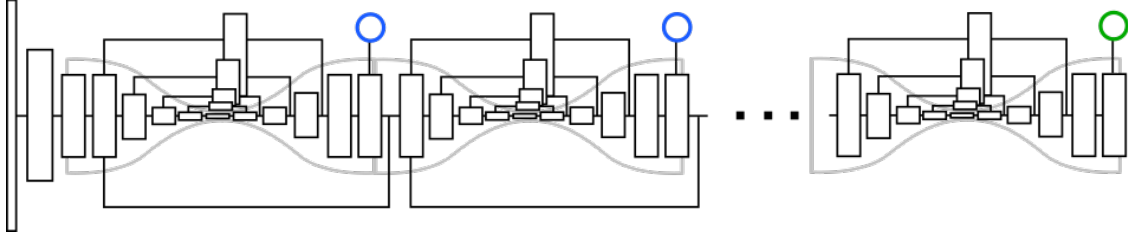
Figure 2. We use the stacked hourglass architecture from Newell et al. [40]. The network performs repeated bottom-up, top-down inference producing a series of intermediate predictions (marked in blue) until the last "hourglass" produces a final result (marked in green). Each box represents a 3x3 convolutional layer. Features are combined across scales by upsampling and performing elementwise addition. The same ground truth is enforced across all predictions made by the network.

heatmaps of object parts. Compared to DeepMask and IS-FCN, our approach is substantially simpler: for each object category we output only two values at each pixel location, a score representing foreground versus background, and a tag representing the identity of an object instance, whereas both DeepMask and IS-FCN produce much higher dimensional output.

3. Approach

3.1. Overview

To introduce associative embedding for joint detection and grouping, we first review the basic formulation of visual detection. Many visual tasks involve detection of a set of visual units. These tasks are typically formulated as scoring of a large set of candidates. For example, single-person human pose estimation can be formulated as scoring candidate body joint detections at all possible pixel locations. Object detection can be formulated as scoring candidate bounding boxes at various pixel locations, scales, and aspect ratios.

The idea of associative embedding is to predict an embedding for each candidate in addition to the detection score. The embeddings serve as tags that encode grouping: detections with similar tags should be grouped together. In multiperson pose estimation, body joints with similar tags should be grouped to form a single person. It is important to note that the absolute values of the tags do not matter, only the distances between tags. That is, a network is free to assign arbitrary values to the tags as long as the values are the same for detections belonging to the same group.

Note that the dimension of the embeddings is not critical. If a network can successfully predict high-dimensional embeddings to separate the detections into groups, it should also be able to learn to project those high-dimensional embeddings to lower dimensions, as long as there is enough network capacity. In practice we have found that 1D embedding is sufficient for multiperson pose estimation, and higher dimensions do not lead to significant improvement. Thus throughout this paper we assume 1D embeddings.

To train a network to predict the tags, we enforce a

loss that encourages similar tags for detections from the same group and different tags for detections across different groups. Specifically, this tagging loss is enforced on candidate detections that coincide with the ground truth. We compare pairs of detections and define a penalty based on the relative values of the tags and whether the detections should be from the same group.

3.2. Stacked Hourglass Architecture

In this work we combine associative embedding with the stacked hourglass architecture [40], a model for dense pixelwise prediction that consists of a sequence of modules each shaped like an hourglass (Fig. 2). Each "hourglass" has a standard set of convolutional and pooling layers that process features down to a low resolution capturing the full context of the image. Then, these features are upsampled and gradually combined with outputs from higher and higher resolutions until reaching the final output resolution. Stacking multiple hourglasses enables repeated bottom-up and top-down inference to produce a more accurate final prediction. We refer the reader to [40] for more details of the network architecture.

The stacked hourglass model was originally developed for single-person human pose estimation. The model outputs a heatmap for each body joint of a target person. Then, the pixel with the highest heatmap activation is used as the predicted location for that joint. The network is designed to consolidate global and local features which serves to capture information about the full structure of the body while preserving fine details for precise localization. This balance between global and local features is just as important in other pixel-wise prediction tasks, and we therefore apply the same network towards both multiperson pose estimation and instance segmentation.

We make some slight modifications to the network architecture. We increase the number of ouput features at each drop in resolution (256 -> 386 -> 512 -> 768). In addition, individual layers are composed of 3x3 convolutions instead of residual modules, the shortcut effect to ease training is still present from the residual links across each hourglass as
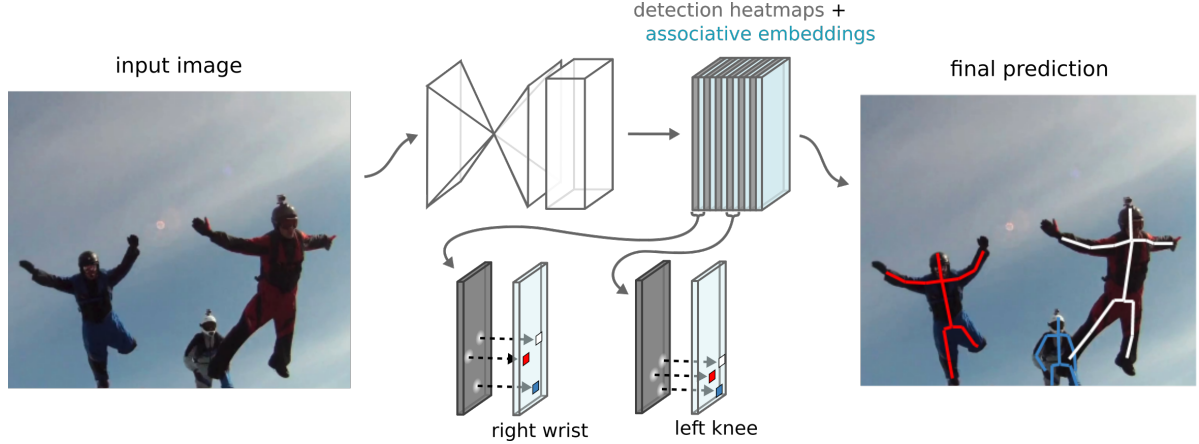
Figure 3. An overview of our approach for producing multi-person pose estimates. For each joint of the body, the network simultaneously produces detection heatmaps and predicts associative embedding tags. We take the top detections for each joint and match them to other detections that share the same embedding tag to produce a final set of individual pose predictions.

well as the skip connections at each resolution.

3.3. Multiperson Pose Estimation

To apply associative embedding to multiperson pose estimation, we train the network to detect joints as performed in single-person pose estimation [40]. We use the stacked hourglass model to predict a detection score at each pixel location for each body joint ("left wrist", "right shoulder", etc.) regardless of person identity. The difference from single-person pose being that an ideal heatmap for multiple people should have multiple peaks (e.g. to identify multiple left wrists belonging to different people), as opposed to just a single peak for a single target person.

In addition to producing the full set of keypoint detections, the network automatically groups detections into individual poses. To do this, the network produces a tag at each pixel location for each joint. In other words, each joint heatmap has a corresponding "tag" heatmap. So, if there are m body joints to predict then the network will output a total of $2m$ channels, m for detection and m for grouping. To parse detections into individual people, we use non-maximum suppression to get the peak detections for each joint and retrieve their corresponding tags at the same pixel location (illustrated in Fig. 3). We then group detections across body parts by comparing the tag values of detections and matching up those that are close enough. A group of detections now forms the pose estimate for a single person.

To train the network, we impose a detection loss and a grouping loss on the output heatmaps. The detection loss computes mean square error between each predicted detection heatmap and its "ground truth" heatmap which consists of a 2D gaussian activation at each keypoint location. This loss is the same as the one used by Newell et al. [40].

The grouping loss assesses how well the predicted tags agree with the ground truth grouping. Specifically, we re-trieve the predicted tags for all body joints of all people at their ground truth locations; we then compare the tags within each person and across people. Tags within a person should be the same, while tags across people should be different.

Rather than enforce the loss across all possible pairs of keypoints, we produce a reference embedding for each person. This is done by taking the mean of the output embeddings of the person's joints. Within an individual, we compute the squared distance between the reference embedding and the predicted embedding for each joint. Then, between pairs of people, we compare their reference embeddings to each other with a penalty that drops exponentially to zero as the distance between the two tags increases.

Formally, let $h_k \in R^{W \times H}$ be the predicted tagging heatmap for the k-th body joint, where $h(x)$ is a tag value at pixel location x. Given N people, let the ground truth body joint locations be $T = \{(x_{nk})\}, n = 1, \ldots, N, k = 1 \ldots, K$, where x_{nk} is the ground truth pixel location of the k-th body joint of the n-th person.

Assuming all K joints are annotated, the reference embedding for the nth person would be

$$\bar{h}_n = \frac{1}{K} \sum_k h_k(x_{nk})$$

The grouping loss L_g is then defined as

$$L_g(h, T) = \frac{1}{N} \sum_n \sum_k \left(\bar{h}_n - h_k(x_{nk},) \right)^2$$
$$+ \frac{1}{N^2} \sum_n \sum_{n'} \exp\{-\frac{1}{2\sigma^2} \left(\bar{h}_n - \bar{h}_{n'} \right)^2\},$$

To produce a final set of predictions we iterate through each joint one by one. An ordering is determined by first considering joints around the head and torso and gradually

Figure 4. Tags produced by our network on a held-out validation image from the MS-COCO training set. The tag values are already well separated and decoding the groups is straightforward.

moving out to the limbs. We start with our first joint and take all activations above a certain threshold after non-maximum suppression. These form the basis for our initial pool of detected people.

We then consider the detections of a subsequent joint. We compare the tags from this joint to the tags of our current pool of people, and try to determine the best matching between them. Two tags can only be matched if they fall within a specific threshold. In addition, we want to prioritize matching of high confidence detections. We thus perform a maximum matching where the weighting is determined by both the tag distance and the detection score. If any new detection is not matched, it is used to start a new person instance. This accounts for cases where perhaps only a leg or hand is visible for a particular person.

We loop through each joint of the body until every detection has been assigned to a person. No steps are taken to ensure anatomical correctness or reasonable spatial relationships between pairs of joints. To give an impression of the types of tags produced by the network and the trivial nature of grouping we refer to Figure 4.

While it is feasible to train a network to make pose predictions for people of all scales, there are some drawbacks. Extra capacity is required of the network to learn the necessary scale invariance, and the precision of predictions for small people will suffer due to issues of low resolution after pooling. To account for this, we evaluate images at test time at multiple scales. There are a number of potential ways to use the output from each scale to produce a final set of pose predictions. For our purposes, we take the produced heatmaps and average them together. Then, to combine tags across scales, we concatenate the set of tags at a pixel location into a vector $v \in R^m$ (assuming m scales). The decoding process does not change from the method described with scalar tag values, we now just compare vector distances.
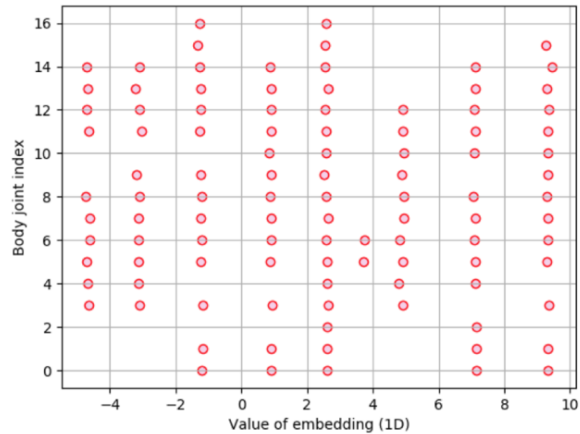

Figure 5. To produce instance segmentations we decode the network output as follows: First we threshold on the detection heatmap, the resulting binary mask is used to get a set of tag values. By looking at the distribution of tags we can determine identifier tags for each instance and match the tag of each activated pixel to the closest identifier.

3.4. Instance Segmentation

The goal of instance segmentation is to detect and classify object instances while providing a segmentation mask for each object. As a proof of concept we show how to apply our approach to this problem, and demonstrate preliminary results. Like multi-person pose estimation, instance segmentation is a problem of joint detection and grouping. Pixels belonging to an object class are detected, and then those associated with a single object are grouped together. For simplicity the following description of our approach assumes only one object category.

Given an input image, we use a stacked hourglass network to produce two heatmaps, one for detection and one for tagging. The detection heatmap gives a detection score at each pixel indicating whether the pixel belongs to *any* instance of the object category, that is, the detection heatmap segments the foreground from background. At the same time, the tagging heatmap tags each pixel such that pixels belonging to the same object instance have similar tags.

To train the network, we supervise the detection heatmap by comparing the predicted heatmap with the ground truth

Figure 6. Qualitative pose estimation results on MSCOCO validation images

heatmap (the union of all instance masks). The loss is the mean squared error between the two heatmaps. We supervise the tagging heatmap by imposing a loss that encourages the tags to be similar within an object instance and different across instances. The formulation of the loss is similar to that for multiperson pose. There is no need to do a comparison of every pixel in an instance segmentation mask. Instead we randomly sample a small set of pixels from each object instance and do pairwise comparisons across the group of sampled pixels.

Formally, let $h \in R^{W \times H}$ be a predicted $W \times H$ tagging heatmap. Let x denote a pixel location and $h(x)$ the tag at the location, and let $S_n = x_{kn}, k = 1, \ldots, K$ be a set of locations randomly sampled within the n-th object instance. The grouping loss L_g is defined as

$$L_g(h, T) = \sum_n \sum_{x \in S_n} \sum_{x' \in S_n} (h(x) - h(x'))^2$$
$$+ \sum_n \sum_{n'} \sum_{x \in S_n} \sum_{x' \in S_{n'}} \exp\{-\frac{1}{2\sigma^2}(h(x) - h(x'))^2\}$$

To decode the output of the network, we first threshold on the detection channel heatmap to produce a binary mask.

Then, we look at the distribution of tags within this mask. We calculate a histogram of the tags and perform non-maximum suppression to determine a set of values to use as identifiers for each object instance. Each pixel from the detection mask is then assigned to the object with the closest tag value. See Figure 5 for an illustration of this process.

Note that it is straightforward to generalize from one object category to multiple: we simply output a detection heatmap and a tagging heatmap for each object category. As with multi-person pose, the issue of scale invariance is worth consideration. Rather than train a network to recognize the appearance of an object instance at every possible scale, we evaluate at multiple scales and combine predictions in a similar manner to that done for pose estimation.

4. Experiments

4.1. Multiperson Pose Estimation

Dataset We evaluate on two datasets: MS-COCO [35] and MPII Human Pose [3]. MPII Human Pose consists of about 25k images and contains around 40k total annotated people (three-quarters of which are available for training). Eval-

Figure 7. Here we visualize the associative embedding channels for different joints. The change in embedding predictions across joints is particularly apparent in these examples where there is significant overlap of the two target figures.

	Head	Shoulder	Elbow	Wrist	Hip	Knee	Ankle	Total
Iqbal&Gall, ECCV16 [29]	58.4	53.9	44.5	35.0	42.2	36.7	31.1	43.1
Insafutdinov et al., ECCV16 [28]	78.4	72.5	60.2	51.0	57.2	52.0	45.4	59.5
Insafutdinov et al., arXiv16a [45]	89.4	84.5	70.4	59.3	68.9	62.7	54.6	70.0
Levinkov et al., CVPR17 [33]	89.8	85.2	71.8	59.6	71.1	63.0	53.5	70.6
Insafutdinov et al., CVPR17 [27]	88.8	87.0	75.9	64.9	74.2	68.8	60.5	74.3
Cao et al., CVPR17 [6]	91.2	87.6	77.7	66.8	75.4	68.9	61.7	75.6
Fang et al., arXiv17 [15]	88.4	86.5	78.6	**70.4**	74.4	**73.0**	**65.8**	76.7
Our method	**92.1**	**89.3**	**78.9**	69.8	**76.2**	71.6	64.7	**77.5**

Table 1. Results (AP) on MPII Multi-Person.

uation is performed on MPII Multi-Person, a set of 1758 groups of multiple people taken from the test set as outlined in [45]. The groups for MPII Multi-Person are usually a subset of the total people in a particular image, so some information is provided to make sure predictions are made on the correct targets. This includes a general bounding box and scale term used to indicate the occupied region. No information is provided on the number of people or the scales of individual figures. We use the evaluation metric outlined by Pishchulin et al. [45] calculating average precision of joint detections.

MS-COCO [35] consists of around 60K training images with more than 100K people with annotated keypoints. We report performance on two test sets, a development test set (test-dev) and a standard test set (test-std). We use the official evaluation metric that reports average precision (AP) and average recall (AR) in a manner similar to object detection except that a score based on keypoint distance is used instead of bounding box overlap. We refer the reader to the MS-COCO website for details [1].

Implementation The network used for this task consists of four stacked hourglass modules, with an input size of 512×512 and an output resolution of 128×128. We train the network using a batch size of 32 with a learning rate of 2e-4

(dropped to 1e-5 after 100k iterations) using Tensorflow [2]. The associative embedding loss is weighted by a factor of 1e-3 relative to the MSE loss of the detection heatmaps. The loss is masked to ignore crowds with sparse annotations. At test time an input image is run at multiple scales; the output detection heatmaps are averaged across scales, and the tags across scales are concatenated into higher dimensional tags. Since the metrics of MPII and MS-COCO are both sensitive to the precise localization of keypoints, following prior work [6], we apply a single-person pose model [40] trained on the same dataset to further refine predictions.

MPII Results Average precision results can be seen in Table 1 demonstrating an improvement over state-of-the-art methods in overall AP. Associative embedding proves to be an effective method for teaching the network to group keypoint detections into individual people. It requires no assumptions about the number of people present in the image, and also offers a mechanism for the network to express confusion of joint assignments. For example, if the same joint of two people overlaps at the exact same pixel location, the predicted associative embedding will be a tag somewhere between the respective tags of each person.

We can get a better sense of the associative embedding output with visualizations of the embedding heatmap (Figure

	AP	AP^{50}	AP^{75}	AP^M	AP^L	AR	AR^{50}	AR^{75}	AR^M	AR^L
CMU-Pose [6]	0.611	0.844	0.667	0.558	0.684	0.665	0.872	0.718	0.602	0.749
G-RMI [42]	0.643	0.846	0.704	**0.614**	0.696	0.698	0.885	0.755	0.644	0.771
Our method	**0.663**	**0.865**	**0.727**	0.613	**0.732**	**0.715**	**0.897**	**0.772**	**0.662**	**0.787**

Table 2. Results on MS-COCO **test-std**, excluding systems trained with external data.

	AP	AP^{50}	AP^{75}	AP^M	AP^L	AR	AR^{50}	AR^{75}	AR^M	AR^L
CMU-Pose [6]	0.618	0.849	0.675	0.571	0.682	0.665	0.872	0.718	0.606	0.746
Mask-RCNN [25]	0.627	**0.870**	0.684	0.574	0.711	–	–	–	–	–
G-RMI [42]	0.649	0.855	0.713	**0.623**	0.700	0.697	0.887	0.755	0.644	0.771
Our method	**0.655**	0.868	**0.723**	0.606	**0.726**	**0.702**	**0.895**	**0.760**	**0.646**	**0.781**

Table 3. Results on MS-COCO **test-dev**, excluding systems trained with external data.

7). We put particular focus on the difference in the predicted embeddings when people overlap heavily as the severe occlusion and close spacing of detected joints make it much more difficult to parse out the poses of individual people.

MS-COCO Results Table 2 and Table 3 report our results on MS-COCO. We report results on both test-std and test-dev because not all recent methods report on test-std. We see that on both sets we achieve the state of the art performance. An illustration of the network's predictions can be seen in Figure 6. Typical failure cases of the network stem from overlapping and occluded joints in cluttered scenes. Table 4 reports performance of ablated versions of our full pipeline, showing the contributions from applying our model at multiple scales and from further refinement using a single-person pose estimator. We see that simply applying our network at multiple scales already achieves competitive performance against prior state of the art methods, demonstrating the effectiveness of our end-to-end joint detection and grouping.

We also perform an additional experiment on MS-COCO to gauge the relative difficulty of detection versus grouping, that is, which part is the main bottleneck of our system. We evaluate our system on a held-out set of 500 training images. In this evaluation, we replace the predicted detections with the ground truth detections but still use the predicted tags. Using the ground truth detections improves AP from 59.2 to 94.0. This shows that keypoint detection is the main bottleneck of our system, whereas the network has learned to produce high quality grouping. This fact is also supported by qualitative inspection of the predicted tag values, as shown in Figure 4, from which we can see that the tags are well separated and decoding the grouping is straightforward.

4.2. Instance Segmentation

Dataset For evaluation we use the val split of PASCAL VOC 2012 [13] consisting of 1,449 images. Additional pretraining is done with images from MS COCO [35]. Evaluation is done using mean average precision of instance

	AP	AP^{50}	AP^{75}	AP^M	AP^L
single scale	0.566	0.818	0.618	0.498	0.670
single scale + refine	0.628	0.846	0.692	0.575	0.706
multi scale	0.630	0.857	0.689	0.580	0.704
multi scale + refine	0.655	0.868	0.723	0.606	0.726

Table 4. Effect of multi-scale evaluation and single person refinement on MS-COCO **test-dev**.

segments at different IOU thresholds. [22, 10, 36]

Implementation The network is trained in Torch [9] with an input resolution of 256×256 and output resolution of 64×64. The weighting of the associative embedding loss is lowered to 1e-4. During training, to account for scale, only objects that appear within a certain size range ar supervised, and a loss mask is used to ignore objects that are too big or too small. In PASCAL VOC ignore regions are also defined at object boundaries, and we include these in the loss mask. Training is done from scratch on MS COCO for three days, and then fine tuned on PASCAL VOC $train$ for 12 hours. At test time the image is evaluated at 3-scales (x0.5, x1.0, and x1.5). Rather than average heatmaps we generate instance proposals at each scale and do non-maximum suppression to remove overlapping proposals across scales. A more sophisticated approach for multi-scale evaluation is worth further exploration.

Results We show mAP results on the val set of PASCAL VOC 2012 in Table 4.2 along with some qualitative examples in Figure 8. We offer these results as a proof of concept that associative embeddings can be used in this manner. We achieve reasonable instance segmentation predictions using the supervision as we use for multi-person pose. Tuning of training and postprocessing will likely improve performance, but the main takeaway is that associative embedding serves well as a general technique for disparate computer vision tasks that fall under the umbrella of detection and grouping problems.
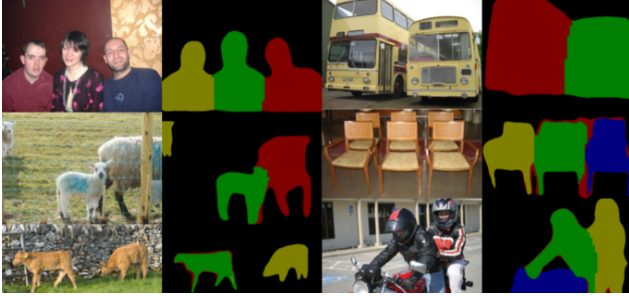
Figure 8. Example instance predictions produced by our system on the PASCAL VOC 2012 validation set.

	IOU=0.5	IOU=0.7
SDS [22]	49.7	25.3
Hypercolumn [23]	60.0	40.4
CFM [11]	60.7	39.6
MPA [36]	61.8	–
MNC [12]	63.5	41.5
Our method	35.1	26.0

Table 5. Semantic instance segmentation results (mAP) on PASCAL VOC 2012 validation images.

5. Conclusion

In this work we introduce associative embeddings to supervise a convolutional neural network such that it can simultaneously generate and group detections. We apply this method to two vision problems: multi-person pose and instance segmentation. We demonstrate the feasibility of training for both tasks, and for pose we achieve state-of-the-art performance. Our method is general enough to be applied to other vision problems as well, for example multi-object tracking in video. The associative embedding loss can be implemented given any network that produces pixelwise predictions, so it can be easily integrated with other state-of-the-art architectures.

References

[1] COCO: Common Objects in Context. http://mscoco.org/home/.

[2] Martín Abadi, Ashish Agarwal, Paul Barham, Eugene Brevdo, Zhifeng Chen, Craig Citro, Greg S. Corrado, Andy Davis, Jeffrey Dean, Matthieu Devin, Sanjay Ghemawat, Ian Goodfellow, Andrew Harp, Geoffrey Irving, Michael Isard, Yangqing Jia, Rafal Jozefowicz, Lukasz Kaiser, Manjunath Kudlur, Josh Levenberg, Dan Mané, Rajat Monga, Sherry Moore, Derek Murray, Chris Olah, Mike Schuster, Jonathon Shlens, Benoit Steiner, Ilya Sutskever, Kunal Talwar, Paul Tucker, Vincent Vanhoucke, Vijay Vasudevan, Fernanda Viégas, Oriol Vinyals, Pete Warden, Martin Wattenberg, Martin Wicke, Yuan Yu, and Xiaoqiang Zheng. TensorFlow: Large-scale machine learning on heterogeneous systems, 2015. Software available from tensorflow.org.

[3] Mykhaylo Andriluka, Leonid Pishchulin, Peter Gehler, and Bernt Schiele. 2d human pose estimation: New benchmark and state of the art analysis. In *Computer Vision and Pattern Recognition (CVPR), 2014 IEEE Conference on*, pages 3686–3693. IEEE, 2014.

[4] Vasileios Belagiannis and Andrew Zisserman. Recurrent human pose estimation. *arXiv preprint arXiv:1605.02914*, 2016.

[5] Adrian Bulat and Georgios Tzimiropoulos. Human pose estimation via convolutional part heatmap regression. In *ECCV*, 2016.

[6] Zhe Cao, Tomas Simon, Shih-En Wei, and Yaser Sheikh. Realtime multi-person 2d pose estimation using part affinity fields. *arXiv preprint arXiv:1611.08050*, 2016.

[7] Joao Carreira, Pulkit Agrawal, Katerina Fragkiadaki, and Jitendra Malik. Human pose estimation with iterative error feedback. In *Proceedings of the IEEE Conference on Computer Vision and Pattern Recognition*, pages 4733–4742, 2016.

[8] Xiao Chu, Wei Yang, Wanli Ouyang, Cheng Ma, Alan L Yuille, and Xiaogang Wang. Multi-context attention for human pose estimation. *arXiv preprint arXiv:1702.07432*, 2017.

[9] Ronan Collobert, Koray Kavukcuoglu, and Clément Farabet. Torch7: A matlab-like environment for machine learning. In *BigLearn, NIPS Workshop*, 2011.

[10] Jifeng Dai, Kaiming He, Yi Li, Shaoqing Ren, and Jian Sun. Instance-sensitive fully convolutional networks. *arXiv preprint arXiv:1603.08678*, 2016.

[11] Jifeng Dai, Kaiming He, and Jian Sun. Convolutional feature masking for joint object and stuff segmentation. In *Proceedings of the IEEE Conference on Computer Vision and Pattern Recognition*, pages 3992–4000, 2015.

[12] Jifeng Dai, Kaiming He, and Jian Sun. Instance-aware semantic segmentation via multi-task network cascades. *arXiv preprint arXiv:1512.04412*, 2015.

[13] Mark Everingham, SM Ali Eslami, Luc Van Gool, Christopher KI Williams, John Winn, and Andrew Zisserman. The pascal visual object classes challenge: A retrospective. *International Journal of Computer Vision*, 111(1):98–136, 2015.

[14] Xiaochuan Fan, Kang Zheng, Yuewei Lin, and Song Wang. Combining local appearance and holistic view: Dual-source deep neural networks for human pose estimation. In *Proceedings of the IEEE Conference on Computer Vision and Pattern Recognition*, pages 1347–1355, 2015.

[15] Haoshu Fang, Shuqin Xie, Yuwing Tai, and Cewu Lu. Rmpe: Regional multi-person pose estimation. *arXiv preprint arXiv:1612.00137*, 2016.

[16] Andrea Frome, Greg S Corrado, Jon Shlens, Samy Bengio, Jeff Dean, Tomas Mikolov, et al. Devise: A deep visual-semantic embedding model. In *Advances in neural information processing systems*, pages 2121–2129, 2013.

[17] Andrea Frome, Yoram Singer, Fei Sha, and Jitendra Malik. Learning globally-consistent local distance functions for

shape-based image retrieval and classification. In *2007 IEEE 11th International Conference on Computer Vision*, pages 1–8. IEEE, 2007.

[18] Ross Girshick, Forrest Iandola, Trevor Darrell, and Jitendra Malik. Deformable part models are convolutional neural networks. In *Proceedings of the IEEE Conference on Computer Vision and Pattern Recognition*, pages 437–446, 2015.

[19] G. Gkioxari, A. Toshev, and N. Jaitly. Chained predictions using convolutional neural networks. In *arXiv preprint arXiv:1605.02346*, 2016.

[20] Yunchao Gong, Liwei Wang, Micah Hodosh, Julia Hockenmaier, and Svetlana Lazebnik. Improving image-sentence embeddings using large weakly annotated photo collections. In *European Conference on Computer Vision*, pages 529–545. Springer, 2014.

[21] Feng Han and Song-Chun Zhu. Bottom-up/top-down image parsing with attribute grammar. *IEEE Transactions on Pattern Analysis and Machine Intelligence*, 31(1):59–73, 2009.

[22] Bharath Hariharan, Pablo Arbeláez, Ross Girshick, and Jitendra Malik. Simultaneous detection and segmentation. In *European Conference on Computer Vision*, pages 297–312. Springer, 2014.

[23] Bharath Hariharan, Pablo Arbeláez, Ross Girshick, and Jitendra Malik. Hypercolumns for object segmentation and fine-grained localization. In *Proceedings of the IEEE Conference on Computer Vision and Pattern Recognition*, pages 447–456, 2015.

[24] Adam W Harley, Konstantinos G Derpanis, and Iasonas Kokkinos. Learning dense convolutional embeddings for semantic segmentation. In *International Conference on Learning Representations (Workshop)*, 2016.

[25] Kaiming He, Georgia Gkioxari, Piotr Dollár, and Ross Girshick. Mask r-cnn. *arXiv preprint arXiv:1703.06870*, 2017.

[26] Peiyun Hu and Deva Ramanan. Bottom-up and top-down reasoning with hierarchical rectified gaussians. In *Proceedings of the IEEE Conference on Computer Vision and Pattern Recognition*, pages 5600–5609, 2016.

[27] Eldar Insafutdinov, Mykhaylo Andriluka, Leonid Pishchulin, Siyu Tang, Bjoern Andres, and Bernt Schiele. Articulated multi-person tracking in the wild. *arXiv preprint arXiv:1612.01465*, 2016.

[28] Eldar Insafutdinov, Leonid Pishchulin, Bjoern Andres, Mykhaylo Andriluka, and Bernt Schiele. Deepercut: A deeper, stronger, and faster multi-person pose estimation model. In *European Conference on Computer Vision (ECCV)*, May 2016.

[29] Umar Iqbal and Juergen Gall. Multi-person pose estimation with local joint-to-person associations. *arXiv preprint arXiv:1608.08526*, 2016.

[30] Andrej Karpathy and Li Fei-Fei. Deep visual-semantic alignments for generating image descriptions. In *Proceedings of the IEEE Conference on Computer Vision and Pattern Recognition*, pages 3128–3137, 2015.

[31] Vladlen Koltun. Efficient inference in fully connected crfs with gaussian edge potentials. *Adv. Neural Inf. Process. Syst*, 2011.

[32] Quoc V Le and Tomas Mikolov. Distributed representations of sentences and documents. In *ICML*, volume 14, pages 1188–1196, 2014.

[33] Evgeny Levinkov, Jonas Uhrig, Siyu Tang, Mohamed Omran, Eldar Insafutdinov, Alexander Kirillov, Carsten Rother, Thomas Brox, Bernt Schiele, and Bjoern Andres. Joint graph decomposition & node labeling: Problem, algorithms, applications. In *IEEE Conference on Computer Vision and Pattern Recognition (CVPR)*, 2017.

[34] Ita Lifshitz, Ethan Fetaya, and Shimon Ullman. Human pose estimation using deep consensus voting. In *European Conference on Computer Vision*, pages 246–260. Springer, 2016.

[35] Tsung-Yi Lin, Michael Maire, Serge Belongie, James Hays, Pietro Perona, Deva Ramanan, Piotr Dollár, and C Lawrence Zitnick. Microsoft coco: Common objects in context. In *European Conference on Computer Vision*, pages 740–755. Springer, 2014.

[36] Shu Liu, Xiaojuan Qi, Jianping Shi, Hong Zhang, and Jiaya Jia. Multi-scale patch aggregation (mpa) for simultaneous detection and segmentation. In *The IEEE Conference on Computer Vision and Pattern Recognition (CVPR)*, June 2016.

[37] Michael Maire. Simultaneous segmentation and figure/ground organization using angular embedding. In *European Conference on Computer Vision*, pages 450–464. Springer, 2010.

[38] Michael Maire, X Yu Stella, and Pietro Perona. Object detection and segmentation from joint embedding of parts and pixels. In *2011 International Conference on Computer Vision*, pages 2142–2149. IEEE, 2011.

[39] Tomas Mikolov, Ilya Sutskever, Kai Chen, Greg S Corrado, and Jeff Dean. Distributed representations of words and phrases and their compositionality. In *Advances in neural information processing systems*, pages 3111–3119, 2013.

[40] Alejandro Newell, Kaiyu Yang, and Jia Deng. Stacked hourglass networks for human pose estimation. *ECCV*, 2016.

[41] Guanghan Ning, Zhi Zhang, and Zhihai He. Knowledge-guided deep fractal neural networks for human pose estimation. *arXiv preprint arXiv:1705.02407*, 2017.

[42] George Papandreou, Tyler Zhu, Nori Kanazawa, Alexander Toshev, Jonathan Tompson, Chris Bregler, and Kevin Murphy. Towards accurate multi-person pose estimation in the wild. *arXiv preprint arXiv:1701.01779*, 2017.

[43] Pedro O Pinheiro, Ronan Collobert, and Piotr Dollar. Learning to segment object candidates. In *Advances in Neural Information Processing Systems*, pages 1990–1998, 2015.

[44] Leonid Pishchulin, Mykhaylo Andriluka, Peter Gehler, and Bernt Schiele. Poselet conditioned pictorial structures. In *Proceedings of the IEEE Conference on Computer Vision and Pattern Recognition*, pages 588–595, 2013.

[45] Leonid Pishchulin, Eldar Insafutdinov, Siyu Tang, Bjoern Andres, Mykhaylo Andriluka, Peter Gehler, and Bernt Schiele. Deepcut: Joint subset partition and labeling for multi person pose estimation. In *IEEE Conference on Computer Vision and Pattern Recognition (CVPR)*, June 2016.

[46] Jianbo Shi and Jitendra Malik. Normalized cuts and image segmentation. *IEEE Transactions on pattern analysis and machine intelligence*, 22(8):888–905, 2000.

[47] X Yu Stella. Angular embedding: from jarring intensity differences to perceived luminance. In *Computer Vision and Pattern Recognition, 2009. CVPR 2009. IEEE Conference on*, pages 2302–2309. IEEE, 2009.

[48] Jonathan Tompson, Ross Goroshin, Arjun Jain, Yann LeCun, and Christoph Bregler. Efficient object localization using convolutional networks. In *Proceedings of the IEEE Conference on Computer Vision and Pattern Recognition*, pages 648–656, 2015.

[49] Jonathan J Tompson, Arjun Jain, Yann LeCun, and Christoph Bregler. Joint training of a convolutional network and a graphical model for human pose estimation. In *Advances in neural information processing systems*, pages 1799–1807, 2014.

[50] Alexander Toshev and Christian Szegedy. Deeppose: Human pose estimation via deep neural networks. In *Computer Vision and Pattern Recognition (CVPR), 2014 IEEE Conference on*, pages 1653–1660. IEEE, 2014.

[51] Ulrike Von Luxburg. A tutorial on spectral clustering. *Statistics and computing*, 17(4):395–416, 2007.

[52] Shih-En Wei, Varun Ramakrishna, Takeo Kanade, and Yaser Sheikh. Convolutional pose machines. *Computer Vision and Pattern Recognition (CVPR), 2016 IEEE Conference on*, 2016.

[53] Kilian Q Weinberger, John Blitzer, and Lawrence K Saul. Distance metric learning for large margin nearest neighbor classification. In *Advances in neural information processing systems*, pages 1473–1480, 2005.